A HIGH-ORDER LOW-ORDER ALGORITHM WITH EXPONENTIALLY-CONVERGENT MONTE CARLO FOR THERMAL RADIATIVE TRANSFER

Simon R. Bolding and Jim E. Morel

Department of Nuclear Engineering

Texas A&M University

College Station, TX 77843

sbolding@tamu.edu; morel@tamu.edu

Mathew A. Cleveland

Los Alamos National Laboratory

Los Alamos, NM 87545

cleveland@lanl.gov

ABSTRACT

We have implemented a new high-order low-order (HOLO) algorithm for solving thermal radiative transfer problems. The low-order (LO) system is based on spatial and angular moments of the transport equation and a linear-discontinuous finite-element spatial representation, producing equations similar to the standard S_2 equations. The LO solver is fully implicit in time and efficiently resolves the non-linear temperature dependence at each time step. The HO solver utilizes exponentially-convergent Monte Carlo (ECMC) to give a globally accurate solution for the angular intensity to a fixed-source, pure absorber transport problem. This global solution is used to compute consistency terms that require the HO and LO solutions to converge towards the same solution. The use of ECMC allows for the efficient reduction of statistical noise in the MC solution, reducing inaccuracies introduced through the LO consistency terms. We compare results with an implicit Monte Carlo (IMC) code for one-dimensional, gray test problems and demonstrate the efficiency of ECMC over standard Monte Carlo in this algorithm.

Key Words: hybrid Monte Carlo, residual Monte Carlo, thermal radiative transfer, high order low order

1. INTRODUCTION

We have implemented a high-order low-order (HOLO) algorithm for the case of 1D gray thermal radiative transfer (TRT) problems. The governing equations are the radiation and material energy balance equations, i.e.,

$$\frac{1}{c}\frac{\partial I}{\partial t} + \mu\frac{\partial I}{\partial x} + \sigma_t I = \frac{\sigma_s}{2}\phi + \frac{1}{2}\sigma_a a c T^4 \tag{1}$$

$$\rho c_v \frac{\partial T}{\partial t} = \sigma_a \phi - \sigma_a a c T^4. \tag{2}$$

In the above equations x is the position, t is the time, μ is the x-direction cosine of the angular intensity $I(x, \mu, t)$, and a, c, ρ, and c_v are the radiation constant, speed of light, mass density, and specific heat; σ_a, σ_s, and σ_t are the absorption, scattering, and total opacities (cm^{-1}), respectively. The desired fundamental unknowns are the material temperature $T(x, t)$ and the scalar radiation intensity $\phi(x, t) = \int_{-1}^{1} I(x, \mu, t)\mathrm{d}\mu$. The equations are strongly coupled through the gray Planckian emission source $\sigma_a a c T^4$, which is a nonlinear function of temperature, and the absorption term $\sigma_a \phi$. In general, the material properties are a function of T, introducing additional non-linearity. The temperature dependent material properties and absorption-reemission physics lead to systems that require solution in a mix of streaming and optically-thick, diffusive regions.

Monte Carlo (MC) solution to the TRT equations is typically achieved by the implicit Monte Carlo (IMC) method, first introduced by Fleck and Cummings [1]. This method linearizes the emission source in time to eliminate the material temperature from the transport equation. The remaining transport equation contains an approximate emission source, as well as an effective scattering cross section representing absorption and reemission over a time step. In optically thick regions, or for large time steps, the effective scattering dominates interactions. In these diffusive regions IMC becomes computationally expensive. Acceleration methods typically attempt to improve efficiency by allowing particles to take discrete steps through optically thick regions based on a discrete diffusion approximation [2,3]. In IMC the approximate linearization of the emission source is not iterated on within a time step, imposing a limit on the time step size to produce physically accurate results [4].

Moment-based hybrid Monte Carlo (MC) methods provide an alternative solution. Recent work has focused on fixed-point iteration high-order low-order (HOLO) approaches [5–8]. Such methods utilize a low-order (LO) operator based on angular moments of the transport equation, formulated over a coarse spatial mesh. Physics operators that are time consuming for MC to resolve, e.g., absorption-reemission and scattering events, are moved to the LO system. Newton methods allow for non-linearities in the LO equations to be fully resolved efficiently [5]. The high-order (HO) system is defined by Eq. (1), with sources estimated from the LO solution that are truly implicit in time. The HO system is solved via MC to produce a high-fidelity solution for the angular intensity. The MC estimate of the angular intensity is used to estimate consistency terms, present in the LO equations, that require the LO system to preserve the angular accuracy of the MC solution; the HO system does not directly estimate a new material temperature, eliminating stability issues that require linearization of the emission source. However, sufficient MC histories must be performed to eliminate statistical noise in the consistency terms that can contaminate the LO solution.

In this work, we demonstrate the utility of an S_2-like LO operator [9] in conjunction with an exponentially-convergent Monte Carlo (ECMC) method [10] for the HO solver. The ECMC algorithm uses information about the intensity from the previous time step to reduce statistical noise to the same order as the HOLO iteration error with significantly less particle histories than standard MC simulations, with less computational time per history. We have derived the LO operator directly from the transport equation, using a linear-discontinuous (LD) finite-element (FE) spatial discretization, such that the HO and LO solutions are converging towards the same solution. Herein we describe the algorithm and present results for two test problems.

1.1. Overview of the HOLO Algorithm

For simplicity, our HOLO method will use a backwards Euler discretization in time, as well as constant specific heats and cell-wise constant opacities. The time discretized equations are

$$\mu \frac{\partial I^{n+1}}{\partial x} + \left(\sigma_t + \frac{1}{c\Delta t} \right) I^{n+1} = \frac{\sigma_s}{2} \phi^{n+1} + \frac{1}{2} \left(\sigma_a ac T^4 \right)^{n+1} + \frac{I^n}{c\Delta t} \tag{3}$$

$$\rho c_v \frac{T^{n+1} - T^n}{\Delta t} = \sigma_a \phi^{n+1} - \sigma_a ac (T^4)^{n+1}. \tag{4}$$

where Δt is the time step size and the superscript n is used to indicate the n-th time step. The algorithm is formed such that the HO and LO solvers can be iterated between until convergence. It is noted that in IMC the time derivative in Eq. (1) is typically solved continuously. The transport equation is discrete in time to avoid difficulties that would arise in coupling to the fully-discrete LO solver.

In the HOLO context, the LO solver models the physical scattering and resolves the material temperature spatial distribution $T(x)$ at each time step. The LO equations are formed via half-range angular and spatial

moments of Eq. (3) and Eq. (4), formed over a spatial finite element mesh. The LO equations take the same form as those used in the hybrid-S_2 method in [9], with element-averaged consistency parameters that are analogous to a variable Eddington factor. If the angular consistency parameters were estimated exactly, then the LO equations are exact with respect to the chosen spatial discretization. These consistency parameters are lagged in each LO solve, estimated from the previous HO solution for $I^{n+1}(x, \mu)$, as explained below. For the initial LO solve within a time step, the parameters are calculated based on the $I^n(x, \mu)$. The LO equations always conserve energy, independent of the accuracy of the consistency terms.

The solution to the LO system is used to construct a spatially LD representation of the scattering and emission sources on the right hand side of Eq. (3). This defines a fixed-source, pure absorber transport problem for the HO operator. This HO transport problem represents a characteristic method that uses MC to invert the continuous streaming plus removal operator with an LD representation of sources. We will solve this transport problem using ECMC. The output from ECMC is $\tilde{I}(x, \mu)$, a space-angle LD FE projection of the exact solution for $I(x, \mu)$. This projection has minimal statistical noise due to the residual formulation used by the ECMC algorithm. Once computed, $\tilde{I}(x, \mu)$ is used to directly evaluate the necessary LO consistency parameters for the next LO solve. Since there is a global, functional representation of the angular intensity, LO parameters are estimated using quadrature and do not require additional tallies. The HO solution is not used to directly estimate a new temperature at the end of the time step; it is only used to estimate the spatial and angular parameters in the LO solution, which eliminates typical operator splitting stability issues that require linearization of the emission source.

The process of performing subsequential HO and LO solves, within a single time step, can be repeated to obtain an increasingly accurate solution for $\phi^{n+1}(x)$ and $T^{n+1}(x)$. Thus, the HOLO algorithm, for the n-th time step, is

1. Perform a LO solve to produce an initial guess for $T^{n+1,0}(x)$ and $\phi^{n+1,0}(x)$, based on consistency terms estimated with $\tilde{I}^n$.

2. Solve the HO system for $\tilde{I}^{n+1,k+1/2}(x, \mu)$ using ECMC, based on the current LO estimate of the emission and scattering sources.

3. Compute LO consistency parameters with $\tilde{I}^{n+1,k+1/2}$.

4. Solve the LO system using HO consistency parameters to produce a new estimate of $\phi^{n+1,k+1}$ and $T^{n+1,k+1}$.

5. Repeat 2 – 4 until convergence is achieved.

6. Move to the next time step.

where the superscript k denotes an outer HOLO iteration. The convergence criteria is based on successive LO solutions for $\phi^{n+1}(x)$ and $T^{n+1}(x)$. The consistency terms force the HO and LO solutions for $\phi^{n+1}(x)$ to be consistent to the order of the current HOLO iteration error.

2. Forming the Low-Order System

To form the LO system of equations, spatial moments are taken over each spatial cell i:
$x \in [x_{i-1/2}, x_{i+1/2}]$, weighted with the standard linear FE interpolatory basis functions. For example, the L moment operator is defined by

$$\langle \cdot \rangle_{L,i} = \frac{2}{h_i} \int_{x_{i-1/2}}^{x_{i+1/2}} b_{L,i}(x)(\cdot)\mathrm{d}x, \qquad (5)$$

where $h_i = x_{i+1/2} - x_{i-1/2}$ is the width of the spatial element and $b_{L,i}(x) = (x_{i+1/2} - x)/h_i$ is the FE basis function, for cell i, corresponding to position $x_{i-1/2}$. The right moment $\langle \cdot \rangle_R$ is defined with weight function $b_{R,i}(x) = (x - x_{i-1/2})/h_i$. Here, it is noted that $\phi_{L,i}$ and $\phi_{R,i}$ represent the values of the scalar intensity in cell i at $x_{i-1/2}$ and $x_{i+1/2}$ that preserve the zeroth and first spatial moments of $\phi(x)$ over the cell, not to be confused with $\langle \phi \rangle_{L,i}$ and $\langle \phi \rangle_{R,i}$, which represent spatial moments. To reduce the angular dimensionality, positive and negative half-range integrals of the angular intensity are taken. The half-range averages of I are defined as $\phi^+(x) = \int_0^1 I(x, \mu) \mathrm{d}\mu$ and $\phi^-(x) = \int_{-1}^0 I(x, \mu) \mathrm{d}\mu$, respectively. Thus, in terms of half-range quantities, $\phi(x) = \phi^-(x) + \phi^+(x)$.

2.1. Radiation Energy Equations

Pairwise application of the L and R basis moments with the $+$ and $-$ half-range integrals to Eq. (3) ultimately yields four radiation moment equations per cell. As in [9], algebraic manipulation is performed to form intensity-weighted averages of μ, which we call consistency terms. As an example, the final equation resulting from application of the L moment and positive half-range integral is

$$- 2\mu_{i-1/2}^{n+1,+} \phi_{i-1/2}^{n+1,+} + \{\mu\}_{L,i}^{n+1,+} \langle \phi \rangle_{L,i}^{n+1,+} + \{\mu\}_{R,i}^{n+1,+} \langle \phi \rangle_{R,i}^{n+1,+} + \left(\sigma_t^{n+1} + \frac{1}{c\Delta t} \right) h_i \langle \phi \rangle_{L,i}^{n+1,+}$$

$$- \frac{\sigma_s h_i}{2} \left(\langle \phi \rangle_{L,i}^{n+1,+} + \langle \phi \rangle_{L,i}^{n+1,-} \right) = \frac{h_i}{2} \langle \sigma_a^{n+1} acT^{n+1,4} \rangle_{L,i} + \frac{h_i}{c\Delta t} \langle \phi \rangle_{L,i}^{n,+}, \quad (6)$$

where the $\phi_{i-1/2}^+$ and $\mu_{i-1/2}^+$ terms represent face quantities at $x_{i-1/2}$. The negative direction and R moment equations are derived analogously. Opacities are assumed constant over each element, evaluated at the average temperature in the element, i.e., $\sigma_a = \sigma_a([T_{L,i} + T_{R,i}]/2)$, $x \in (x_{i-1/2}, x_{i+1/2})$. The element-averaged angular consistency terms are defined in terms of half-range integrals, e.g.,

$$\{\mu\}_{L,i}^{n+1,+} = \frac{\dfrac{2}{h_i} \int\limits_0^1 \int\limits_{x_{i-1/2}}^{x_{i+1/2}} \mu \, b_{L,i}(x) I^{n+1}(x, \mu) \mathrm{d}x \mathrm{d}\mu}{\dfrac{2}{h_i} \int\limits_0^1 \int\limits_{x_{i-1/2}}^{x_{i+1/2}} b_{L,i}(x) I^{n+1}(x, \mu) \mathrm{d}x \mathrm{d}\mu}. \quad (7)$$

The $\mu_{i-1/2}^{n+1,+}$ term is defined analogously and represents an angular average on the face at $x_{i-1/2}$.

2.2. Material Energy Equations

To derive the LO material energy equations, $T(x)$ is represented spatially in the LD trial space, i.e., $T(x) \simeq T_{L,i} b_{L,i}(x) + T_{R,i} b_{R,i}(x)$, $x \in (x_{i-1/2}, x_{i+1/2})$. Similarly, the emission term is represented in the material and radiation equations with the LD interpolant of $T^4(x)$. The L and R spatial moments are taken of the material energy equation, using the LD definitions for $T(x)$ and $\sigma_a acT^4(x)$ to evaluate and simplify integrals where possible. For example, the final LO material energy equation resulting from application of the L moment is

$$\frac{\rho c_v}{\Delta t} \left[\left(\frac{2}{3} T_{L,i} + \frac{1}{3} T_{R,i} \right)^{n+1} - \left(\frac{2}{3} T_{L,i} + \frac{1}{3} T_{R,i} \right)^n \right] + \sigma_a^{n+1} \left(\langle \phi \rangle_{L,i}^+ + \langle \phi \rangle_{R,i}^- \right)^{n+1}$$

$$= \sigma_a^{n+1} ac \left(\frac{2}{3} T_{L,i}^4 + \frac{1}{3} T_{R,i}^4 \right)^{n+1}. \quad (8)$$

Because the material energy balance only contains angularly integrated quantities, there is no need to take angular moments of the above equation.

2.3. Closing the System with Information from the HO solution

The six degrees of freedom (DOF) over each cell i are the four moments $\langle\phi\rangle_{L,i}^+$, $\langle\phi\rangle_{R,i}^+$, $\langle\phi\rangle_{L,i}^-$, and $\langle\phi\rangle_{R,i}^-$ and the two spatial LD edge values $T_{L,i}$ and $T_{R,i}$. The four radiation and two material energy equations define a system of equations for the six DOF, coupled to other cells via upwinding in the streaming term. However, the angular consistency parameters (e.g., Eq. (7)) are not known a priori, and there is no relation between the volume and face averaged quantities. A lagged estimate of I^{n+1} from the previous HO solve is used to estimate the angular consistency parameters. In the HOLO context, the equations for LO unknowns at iteration $k+1$ use consistency parameters computed using (via relations, e.g., Eq. (7)) with the latest HO solution $\tilde{I}^{n+1,k+1/2}$ as an approximation for $I^{n+1}(x,\mu)$. To close the LO system spatially, the usual LD upwinding approximation is used. For example, for positive flow (e.g., Eq. (6)) the face terms $\mu_{i-1/2}$ and $\phi_{i-1/2}$ are upwinded from the previous cell $i-1$ or from a boundary condition; the terms at $x_{i+1/2}$ are linearly extrapolated, computed using the L and R basis moments, e.g., $\phi_{i+1/2}^+ = 2\langle\phi\rangle_R^+ - \langle\phi\rangle_L^+$. Because the HO ECMC solver uses an LD representation, this LO spatial closure is inherently consistent. Because there are no spatial temperature derivatives, there is no evaluation of T at faces and thus no need for an additional closure in T.

The LD closure is not strictly positive. In particular, for optically thick cells with a steep temperature gradient, the solution is driven negative. In thick regions of TRT problems, reasonably fine spatial cells can still be on the order of millions of mean free paths; negativities with a LD representation are unavoidable in practice for such cells and mesh refinement is of minimal use. Typically, for a standard LD FE method, the equations are lumped to produce a strictly positive solution for 1D [11]. However, standard FE lumping procedures would introduce difficulties in computing the consistency terms from the HO solution. Thus, an alternative spatial closure is used that is equivalent to the standard FE lumping procedure. The L and R moments are defined the same as before, preserving the same average within a cell, but the relation between the moments and the outflow is modified. For example, for positive μ, the outflow is now defined as $\phi_{i+1/2}^+ = \langle\phi\rangle_R^+$. Because the basis function $b_{R,i}(x)$ is strictly positive, the outflow is inherently positive. This closure is only used in cells in which negativities occur.

2.4. Solving the Non-Linear LO System

We have used Newton's method to solve the global system of coupled LO equations, based on a typical linearization of the Planckian source with opacities evaluated at lagged temperatures, as described in [11]. Newton iterations are repeated until $\phi^{n+1}(x)$ and $T^{n+1}(x)$ are converged to a desired relative tolerance. The lumping-equivalent discretization discussed above is used for cells where the solution for ϕ^{n+1} becomes negative. When negativities are detected, the lumping-equivalent discretization is used within those cells and that Newton step is repeated.

3. The ECMC High Order Solver

The transport equation to be solved by the HO solver is

$$\mu\frac{\partial I^{n+1,k+1/2}}{\partial x} + \left(\sigma_t^k + \frac{1}{c\Delta t}\right)I^{n+1,k+1/2} = \frac{\sigma_s^k}{2}\phi^{n+1,k} + \frac{1}{2}\left(\sigma_a^k acT^4\right)^{n+1,k} + \frac{\tilde{I}^n}{c\Delta t} \tag{9}$$

where the superscript k represents the outer HOLO iteration index. Material property indices will be suppressed from now on. Here, $k+1/2$ denotes the ECMC solution within outer HOLO iteration k, whereas k and $k+1$ represent successive LO solves. The sources at k are estimated by the previous LO solution. Opacities are evaluated at $T^{n+1,k}$. As all sources on the right side of the equation are known, this defines a fixed-source, pure absorber transport problem. We will solve this equation using ECMC. A more detailed description of the ECMC method can be found in [12], but a brief overview is given here.

In operator notation, the previous equation can be written as

$$\mathbf{L}^k I^{n+1,k+1/2} = q^k \tag{10}$$

where $I^{n+1,k+1/2}$ is the transport solution of the angular intensity based on the k-th LO estimate of q^k. The linear operator $\mathbf{L}^k$ is the streaming plus removal operator defined by the left hand side of Eq. (3). The m-th approximate solution to Eq. (10) (m represents inner HO batches) is represented as $\tilde{I}^{n+1,(m)}$. The m-th residual is defined as $r^{(m)} = q - \mathbf{L}\tilde{I}^{n+1,(m)}$. For reference, the residual at iteration m in the HO solve is

$$r^{(m),k+1/2} = \frac{\sigma_s}{2}\phi^{n+1,k} + \frac{1}{2}\left(\sigma_a acT^4\right)^{n+1,k} + \frac{\tilde{I}^n}{c\Delta t} - \left(\mu\frac{\partial \tilde{I}^{n+1,k+1/2}}{\partial x} + \left(\sigma_t + \frac{1}{c\Delta t}\right)\tilde{I}^{n+1,k+1/2}\right)^{(m)} \tag{11}$$

where the k terms are LD in space on the coarsest mesh and are not recalculated at any point during the HO solve. The functional form of $\tilde{I}^n$ is defined over the finest space-angle mesh from the final HOLO iteration of the previous time step.

To define the ECMC algorithm, the HOLO iteration indices are dropped, as the LO estimated q^k and $\mathbf{L}^k$ remain constant over the entire HO solve. Addition of $\mathbf{L}I^{n+1} - q = 0$ to the residual equation and manipulation of the result yields the error equation

$$\mathbf{L}(I^{n+1} - \tilde{I}^{n+1,(m)}) = \mathbf{L}\tilde{\epsilon}^{(m)} = r^{(m)} \tag{12}$$

where I^{n+1} is the exact solution and $\tilde{\epsilon}^{(m)}$ is finite element representation of the error in $\tilde{I}^{n+1,(m)}$. The $\mathbf{L}$ operator in the above equation is inverted yielding the Monte Carlo estimate of the error in $\tilde{I}^{n+1,(m)}$, i.e.,

$$\tilde{\epsilon}^{(m)} = \mathbf{L}^{-1}r^{(m)} \tag{13}$$

where $\mathbf{L}^{-1}$ is the Monte Carlo inversion of the streaming and removal operator. Here, we emphasize the solution $\tilde{I}^{n+1,(m)}$ represents the projection of the exact Monte Carlo solution onto the trial space. This is in general far more accurate than a standard finite element solution. For example, the LD trial space preserves the zeroth and first spatial moment over a cell; the zeroth moment is computed using a standard path-length volumetric flux tally, which is equivalent to typical volumetric averages computed in Monte Carlo calculations. The primary truncation error is in the LD representation of the right hand side source terms and residual at each iteration. Only volumetric flux tallies over all of the finest space-angle elements are used; tallies are computed for the average, slope in x, and slope in μ of $I^{n+1}(x,\mu)$ by weighting the tallies for I^{n+1} with the appropriate basis function.

The ECMC algorithm is

1. Initialize the guess for $\tilde{I}^{n+1,(0)}$ to $\tilde{I}^n$ or the projection of $\tilde{I}^{n+1}$ from the latest HO solve

2. Compute $r^{(m)}$.

3. Solve $\tilde{\epsilon}^{(m)} = \mathbf{L}^{-1}r^{(m)}$

4. Compute a new estimate of the intensity $\tilde{I}^{n+1,(m+1)} = \tilde{I}^{n+1,(m)} + \tilde{\epsilon}^{(m)}$

5. Repeat steps $2 - 4$ until desired convergence criteria is achieved.

The initial guess for the angular intensity $I^{n+1,(0)}$ is computed based on the previous solution for $\tilde{I}^n$. This is a critical step in the algorithm; it significantly reduces the required number of particles per time step because I does not change drastically between time steps in optically thick regions. It is noted that the

ECMC batch (steps 1-4 of the algorithm) results in essentially the same estimate of the solution as the residual formulation used in [7]. The primary difference is that our method uses an LD trial space, and we are able to use our new estimate of the solution to recompute a residual.

Exponential convergence is obtained because with each batch a better estimate of the solution is being used to compute the new residual, decreasing the magnitude of the Monte Carlo source each iteration m, relative to the solution I^{n+1}. Each Monte Carlo estimate of ϵ still has a computable statistical uncertainty. If the statistical estimate of $\tilde{\epsilon}$ is not sufficiently accurate, then the iterations would diverge. Because the exact angular intensity does not in general lie within the LD trial space, the iterative estimate of the error will eventually stagnate once the error cannot be sufficiently represented by a given FE mesh. Although mesh refinement is not performed in the calculations presented here, an adaptive $h-$refinement algorithm has been implemented that can be used to allow the system to continue converging towards the exact solution.

3.1. Variance Reduction and Source Sampling

As in [6], because we are solving a pure absorber problem with Monte Carlo, we will allow particles to stream without absorption to reduce statistical variance in the tallies. The weight of particles is reduced deterministically along the path as they stream, with no need to sample a path length. Because particles are exponentially attenuated, the normalized weight is adjusted as $w(x) = w(x_0)exp(-|(x - x_0)/\mu|)$, where x_0 is the starting location of the path. The tallies are modified to account for the continuously changing weight. Histories are allowed to stream in this manner for 6 mean free paths before switching to analog path length sampling; this prevents the tracking of very small weight histories.

As another way to improve efficiency and statistics, a modified systematic sampling method [13] was used for determining source particle locations. The goal is to effectively distribute particle histories to regions of importance, but to sample a sufficient number of histories in less probable regions to prevent large statistical noise. However, there is no need to sample histories in regions that are in equilibrium and the solution is not changing over a time step. The residual gives a good indication of where particles are most likely to contribute to the error, particularly in optically thick cells. In the sampling algorithm the number of particle histories sampled in each space-angle cell is predetermined and proportional to the magnitude of the residual in that cell. Then, for the predetermined number of histories within a cell, the source location is randomly sampled according to the residual source distribution within that cell. There is a relative probability cutoff such that cells with an insignificant residual will have no histories sampled there. In these regions the problem is remaining in steady state and the solution is known exactly. For cells that are significant, but have a predetermined number of histories below some preset minimum N_{min}, the number of histories sampled in that cell is set to N_{min}. This is to limit bad statistics in low probability cells, particularly in the case of adaptively refined meshes. In the simulations performed for this work N_{min} is set to one. This is done for comparing to IMC to keep the total number of histories per time step constant throughout the entire simulation.

3.2. Fixup Near the Wave-Front

For the HO solver, in cells near the radiation wave front, the LD trial space results in negativities in $\tilde{I}^{n+1}(x, \mu)$, as with the LO solver. Currently, we do not treat these cells differently for the ECMC solve, but detect if the consistency terms lie in the approprate half space at the end of the HO solve. If the terms are non-physical, then they are set to the corresponding S_2-equivalent value. This may lead to artificially fast wave-speeds in certain cells. Future work will include using a different trial space in these cells that is strictly positive.

4. Results

4.1. Marshak Wave

We will compare results of the HOLO method to IMC with a source tilting algorithm [14]. In IMC the material and radiation energy fields are discretized spatially to solve for cell-averaged values. Inaccurate spatial representation of the emission source over a cell can result in energy propagating through the domain artificially fast, yielding non-physical results referred to as "teleportation error" [15]. The IMC method uses a fixup known as source tilting to mitigate this problem. Source tilting reconstructs a more accurate linear-discontinuous representation of the emission source within a cell based on the cell-averaged material temperatures in adjacent cells. This is not necessary in our method because of the LD representation of the emission source.

For the first problem, the radiation and material energies are initially in equilibrium at 2.5E-05 keV. An isotropic incident intensity of 0.150 keV is applied at $x = 0$; the incident intensity on the right boundary is 2.5E-05 keV. The material properties are $\rho = 1$ g cm^{-3} and $c_v = 0.013784$ jks/keV-g. The absorption cross section varies as $\sigma(T) = 0.001 \, \rho \, T^{-3}$ (cm^{-1}). The simulation was ran for 5 sh (1 sh = 10^{-8} s) with a fixed time step size of 0.001 sh. For comparison purposes, we have not used adaptive mesh refinement, only performed one HOLO iteration per time step, and use a fixed 3 HO batches with equal number of histories per batch. A relative tolerance of 1.E-06 in the norm of $\phi(x)$ and $T(x)$ was used for the LO newton solver. Radiation energy distributions are plotted as an equivalent temperature given by $T_r = \sqrt[4]{\phi/(ac)}$. Cell-averaged quantities are plotted. Although scattering physics can be handled by the LO solver in this method [8], we have only considered pure absorber problems here.
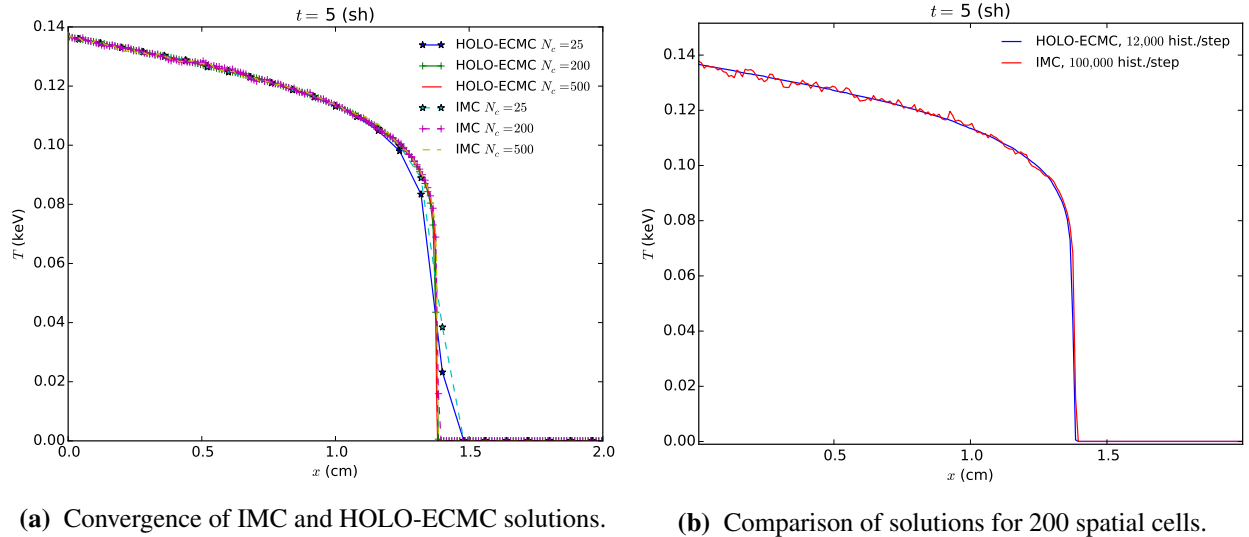

(a) Convergence of IMC and HOLO-ECMC solutions.

(b) Comparison of solutions for 200 spatial cells.

Figure 1: Comparison of solutions for Marshak wave problem at t = 5 sh.

Fig. 1a compares the cell-averaged radiation temperatures for the IMC and HOLO method with ECMC, for various number of spatial mesh cells N_c. For the HOLO solver, we have used 4 equal-sized cells in μ. For the cases of $N_c = 25$ and $N_c = 200$, 4,000 histories per batch (12,000 per time step) were used. For $N_c = 500$, 16,000 histories per batch were used due to increased number of cells that need to be sampled. For all IMC calculations, 10^5 histories per time step were used. The solutions agree as the mesh is converged. There is similar agreement in the location of the wave front due to the linear shape of the emission source over a cell. The cells at the wave front required use of the lumping-equivalent discretization during the LO solve, resulting in strictly positive solutions.

Fig. 1b compares solutions for the case of 200 cells. For the IMC solution 10^5 histories per time step were simulated; for the HOLO method only $4,000$ histories per batch (12,000 per time step) were simulated. There is significant statistical noise in the IMC solution compared to the HOLO solution. The HOLO solution visually demonstrates no statistical noise. The relatively small number of histories is possible due to the residual formulation and the initial guess of $\tilde{I}^n$ for the first HO solve. Since the transport solve is only determining the change over the time step, the statistical noise in the result is small relative to the magnitude of I^{n+1}. Also, the source sampling only places particles in cells where the residual is large. No particles are sampled in the equilibrium region out front of the wave.

We have measured the total CPU time for simulations to provide a crude measure of the computational cost. Absolute comparisons in the computational cost of the two methods are difficult to make ~~due to differences in the codes~~. For instance, the IMC and HOLO methods are implemented in different code infrastructures. Additionally, the HOLO method fully resolves non-linearities at each time step, whereas IMC is using a single linearized step with lagged opacities. A more thorough investigation of efficiency that accounts for statistical error and accuracy over larger time steps will be performed in future work.

Table I compares simulation CPU times for IMC and the HOLO method with ECMC for different numbers of histories per time step. Also given is one case with an increased time step size. The HOLO method does not scale with the number of histories due to the fixed cost of the LO solver. The cost of the LO solver is more significant at 12,000 histories per time step where IMC takes less time, whereas at 10^5 histories the HOLO simulation takes less time. If the large reduction in statistical error by the HOLO method relative to IMC ~~is~~ considered, the gain in efficiency over IMC would be significant. Similar to the results in [6], as the time step size is increased to to 0.005 sh, the IMC method increases in cost (per time step) more than the HOLO method. The increase in the IMC simulation time is due to the increased amount of (expensive) effective scattering events.

Table I: Total CPU time required for the Marshak Wave problem for 200 x cells. Simulation end time is t $= 5$ sh.

Hists. per step	$\Delta t(sh)$	IMC	HOLO-ECMC
10^5	0.001	5190 s	4003 s
1.2×10^4	0.001	635 s	692 s
1.2×10^4	0.005	303 s	179 s

4.2. Two Material Problem

This problem consists of an optically thin (left) and an optically thick (right) material region, with constant opacities. The material properties are given in Table II. Initially the radiation and material energies are in equilibrium at a temperature of 0.05 keV. An isotropic incident intensity of 0.500 keV is applied at $x = 0$ at $t = 0$; the isotropic incident intensity on the right boundary is 0.05 keV. The simulation is ran for 5 sh. For all HOLO simulations, we have used 8 equal-sized mesh cells in μ.

Table II: Material properties for two material problem

	$x \in [0, 0.5)$ cm	$x \in [0.5, 1.0]$ cm
σ_a (cm^{-1})	0.2	2000
ρ (g cm^{-3})	0.01	10.0
c_v (jks/keV-g)	0.1	0.1

(a) Comparison of IMC and HOLO-ECMC.
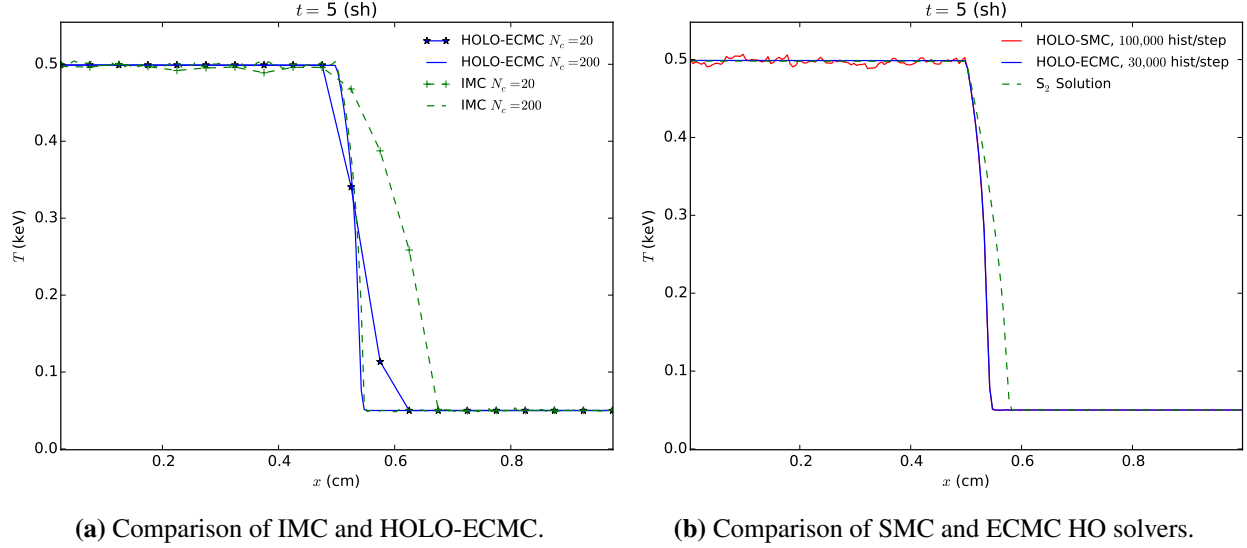
(b) Comparison of SMC and ECMC HO solvers.

Figure 2: Comparison of radiation temperatures for two material problem.

Fig. 2a compares the HOLO and IMC radiation temperatures at the end of the simulation. The IMC method used 10^5 histories per time step, where as the HOLO method used 3×10^4 histories per time step. The IMC and HOLO results show good agreement over the finer mesh. On the coarse mesh ($N_c = 20$), the HOLO method predicts the location of the wave-front more accurately than the IMC method.

Fig. 2b compares results for different HO solvers. The HOLO algoirthm with the ECMC HO solver (HOLO-ECMC) results are for running 3 batches of 10,000 histories, per time step. The solution for the HOLO method with a standard MC solver as the HO solver (HOLO-SMC) with standard source sampling uses 10^5 histories per time step. Also plotted is an S_2 solution obtained by using consistency terms that are equivalent to S_2 and not performing the HO correction step. The HOLO-SMC solution demonstrates significant statistical noise. This noise is introduced into the LO solver by bad statistics in computing the consistency terms. The S_2 solution results in an artificially fast wave front as expected, demonstrating the necessity of HO correction in this problem.

Total CPU times for the two material problem are given in Table III. The end time for the simulations in this table was reduced to 2 sh. The observed behavior in the computational times is similar to those in the first problem. Because the opacities do not have a T^{-3} behavior in this problem, the cost of the effective scattering cross section in IMC is more apparent, resulting in longer simulation times. As the time step size is increased by a factor of 5, the average cost per time step for the simulation increases by a factor of ~ 3.4; for HOLO-ECMC the increase is only ~ 1.1.

Table III: Total CPU time required for the two material problem. Simulation end time is t = 2 sh.

Hists. per step	$\Delta t(sh)$	IMC	HOLO-ECMC
10^5	0.001	3428	673
3×10^4	0.001	1036	397
3×10^4	0.005	699	86

5. Conclusions

We have been able to produce solutions for Marshak wave test problems using a new HOLO method that is in agreement with IMC. Unlike IMC, our method requires no effective scattering events to be included in the MC simulation, limiting the total run time of the simulations. The LD spatial representation mitigates issues with teleportation error, similar to source tilting in the IMC algorithm. The LO solver resolves the non-linearities in the equations resulting in a fully implicit time discretization. The ECMC approach, with initial guesses based on the previous radiation intensity, results in efficient reduction of statistical error and allows for particles to be distributed to largely varying regions of the problem. The LO solver can accurately and efficiently resolve the solution in diffusive regions, while the HO transport solver provides the accuracy of a full transport treatment where necessary.

The primary difficulty to overcome ~~is~~ in the HO solver at the wave front. A strictly positive spatial discretization in the residual formulation needs to be implemented for high accuracy solutions near the wave front. The representation needs to be implemented such that the spatial closure in the LO system is consistent with the HO representation for the solution. The ability to represent the solution accurately in rapidly varying regions of the problem will be key for generalization of this method to higher dimensions. Future work will include comparisons of the HOLO method with IMC using a figure of merit to quantify the efficiency of the simulations when statistical noise is considered; the sensitivity of the method to mesh sizes and time step sizes will be investigated more thoroughly. Ultimately, we will apply this method to multi-group TRT equations, before extending it to multiple spatial dimensions.

ACKNOWLEDGEMENTS

REFERENCES

[1] J. A. Fleck, Jr. and J. D. Cummings, Jr., "An Implicit Monte Carlo Scheme for Calculating Time and Frequency Dependent Nonlinear Radiation Transport," *J. Comput. Phys.*, **8**, 3, pp. 313–342 (Dec. 1971).

[2] N. Gentile, "Implicit Monte Carlo diffusionAn acceleration method for Monte Carlo time-dependent radiative transfer simulations," *Journal of Computational Physics*, **172**, 2, pp. 543–571 (2001).

[3] J. D. Densmore, K. G. Thompson, and T. J. Urbatsch, "A hybrid transport-diffusion Monte Carlo method for frequency-dependent radiative-transfer simulations," *Journal of Computational Physics*, **231**, 20, pp. 6924–6934 (2012).

[4] A. B. Wollaber, E. W. Larsen, and J. D. Densmore, "A Discrete Maximum Principle for the Implicit Monte Carlo Equations," *Nuclear Science and Engineering*, **173**, 3, pp. 259–275 (2013).

[5] J. Willert, C. Kelly, D. Knoll, and H. Park, "A Hybrid Approach to the Neutron Transport k-Eigenvalue Problem using NDA-based Algorithms," (2013), M&C.

[6] H. Park, J. Densmore, A. Wollaber, D. Knoll, and R. Ramenzahn, "Monte Carlo Solution Methods in a Moment-Based Scale-Bridging Algorithm For Thermal Radiative Transfer Problems," M&C (2013).

[7] J. Willert and H. Park, "Residual Monte Carlo High-order Solver for Moment-Based Accelerated Thermal Radiative Transfer Equations," *Journal of Computational Physics*, **276**, pp. 405 – 421 (2014).

[8] S. Bolding and J. Morel, "A High-Order Low-Order Algorithm with Exponentially-Convergent Monte Carlo for k-Eigenvalue problems," ANS Winter Meeting (2014).

[9] E. Wolters, *Hybrid Monte Carlo - Deterministic Neutron Transport Methods Using Nonlinear Functionals*, Ph.D. dissertation, Michigan (2011).

[10] J. Peterson, J. Morel, and J. Ragusa, "Exponentially Convergent Monte Carlo for the 1-D Transport Equation," M&C (2013).

[11] J. Morel, T. Wareing, and K. Smith, "Linear-Discontinuous Spatial Differencing Scheme for S_n Radiative Transfer Calculations," *Journal of Computational Physics*, **128**, pp. 445–462 (1996).

[12] J. Peterson, *Exponentially Convergent Monte Carlo for the 1-D Transport Equation*, Master's thesis, Texas A&M (2014).

[13] J. Shultis and W. Dunn, *Exploring Monte Carlo Methods*, Academic Press, Burlington, MA 01803 (2012).

[14] T. Urbatsch and T. Evans, "Milagro Version 2 An Implicit Monte Carlo Code for Thermal Radiative Transfer: Capabilities, Development, and Usage," Los Alamos National Laboratory Report LA-14195-MS (2006).

[15] M. S. McKinley, E. D. Brooks III, and A. Szoke, "Comparison of implicit and symbolic implicit Monte Carlo line transport with frequency weight vector extension," *Journal of Computational Physics*, **189**, 1, pp. 330–349 (2003).